A New Second-Order Turbulence Closure Scheme for Modeling the Oceanic Mixed Layer

S. J. D. D'ALESSIO,* K. ABDELLA,+ AND N. A. MCFARLANE

Canadian Centre for Climate Modelling and Analysis, University of Victoria, Victoria, British Columbia, Canada

(Manuscript received 28 April 1997, in final form 17 November 1997)

ABSTRACT

A new second-order turbulence closure scheme is proposed for the oceanic mixed layer. The scheme is similar in complexity to a Mellor–Yamada level 2.5 scheme in that the turbulent kinetic energy is the only turbulence quantity treated prognostically with the others determined diagnostically. The main difference lies in the treatment of the turbulent fluxes. While momentum fluxes are assumed to be downgradient, the other turbulent fluxes allow for nonlocal and countergradient contributions. The model was tested against several idealized forcing experiments for wind-deepening, heating and cooling cases, and also against observational data taken from Ocean Weather Stations November and Papa. The simulations reveal good agreement with other models. The present scheme also performs reasonably well in reproducing the observed sea surface temperature and boundary layer depth for the year 1961 at stations November and Papa. Also proposed are ways of incorporating near-surface processes such as Langmuir circulation and wave breaking. Simulations have shown that wave breaking leads to negligible deepening of the mixed layer, while the inclusion of Langmuir circulations causes further deepening to occur.

1. Introduction

In climate modeling it is imperative to include the exchange processes such as heat, momentum, and water vapor between the atmosphere and the ocean. The mixed layer refers to the upper portion of the ocean that is in direct contact with the atmosphere and is usually observed to be thoroughly mixed. It plays an important role in communicating fluxes with the atmosphere and also acts as a link between the atmosphere and the deeper ocean. A means of investigating the response of the mixed layer to a given atmospheric forcing is through the implementation of one-dimensional column models that account for vertical variations. Horizontal variations can be significant under certain conditions and in specific regions; however, their influence is either explicitly specified or omitted in these models.

In column models a set of conservation equations governing the mean horizontal velocity components, temperature, and salinity are driven by fluxes of heat and wind stress imposed by the atmosphere at the ocean surface and are also forced from below due to interior mixing processes. The mixed layer then responds to these forcings through deepening or shallowing and heating or cooling. The resulting sea surface temperature (SST) has a significant impact on the climate and also on the local biological environment. Over the years numerous models have been proposed to simulate the mixed layer. These are generally formulated following one of two common approaches. In bulk models the equations are integrated across the mixed layer on the assumption that the mean quantities are nearly uniform throughout it. This idea was first introduced by Ball (1960) and designed for atmospheric use and was later extended to handle the ocean by Kraus and Turner (1967). In these models the advance and retreat of the mixed layer depends on the parameterizations of the fluxes at its base. Another approach, known as a turbulence closure scheme, attempts to model the various turbulent fluxes appearing in the equations. Here, the equations are dealt with in a differential form rather than an integral form. One is then faced with the task of prescribing the various turbulent fluxes in terms of the prognostic variables.

Presented in this paper is a second-order turbulence closure scheme for the mixed layer. In second-order closure schemes the equations dictating the turbulent fluxes are closed at the second-moment level and thus require the specification of unknown third-moment turbulence quantities. Third-order closure schemes have also been developed by Warn-Varnas and Piacsek (1979) and André and Lacarrère (1985). Unless simplifications

* Current affiliation: Department of Applied Mathematics, University of Waterloo, Waterloo, Ontario, Canada.
+ Current affiliation: Department of Mathematics, Trent University, Peterborough, Ontario, Canada.

Corresponding author address: Dr. S. J. D. D'Alessio, Department of Applied Mathematics, University of Waterloo, Waterloo, Ontario N2L 3G1, Canada.
E-mail: sdalessio@math.uwaterloo.ca

are made, substantial computational demands can be required by turbulence closure schemes since they introduce additional equations for the various second moments that must be solved in conjunction with the usual set for momentum, temperature, and salinity. Realizing this, modelers have proposed schemes to reduce the computational burden. Mellor and Yamada (1974, 1982), for example, introduced a hierarchy of closures using a systematic expansion procedure to analyze the departure from the state of local isotropy. The level 2.5 scheme in this hierarchy has since been used extensively in geophysical applications. In a Mellor–Yamada level 2.5 scheme third moments are either ignored or modeled downgradiently and the only additional equation required is that for the turbulent kinetic energy (TKE). In the present scheme the parameterizations used for the third moments are taken from the recent work of Abdella and McFarlane (1997), which allow for countergradient and nonlocal contributions. Also, as in the Mellor–Yamada level 2.5 scheme, only the TKE is treated prognostically here. By making certain assumptions about the nature of the turbulence, the remaining second moments can be determined diagnostically. The new scheme also offers some physical insight into near-surface processes that are unique to the ocean. An attempt has been made to model the effects of Langmuir circulations and wave breaking, which are probably the most important processes responsible for enhanced mixing in the upper ocean.

Subsequent sections are organized as follows. In section 2 we present the modeling equations along with the forcing conditions and briefly discuss the physics. A means of estimating the boundary layer depth is outlined, while the rational behind the turbulent flux expressions is included in the appendix. Then, in section 3, the performance of the model is addressed. The model is tested against several bulk and turbulence closure schemes for various idealized forcings including wind driven, heating, and cooling cases. Also, the model is tested against observational data taken from Ocean Weather Stations November and Papa. Section 4 is devoted to discussing ways of incorporating near-surface processes such as Langmuir circulation and wave breaking into the model. This is followed by the conclusions.

2. Modeling equations and boundary conditions

The equations governing the mean flow, potential temperature, salinity, and TKE in a horizontally homogeneous ocean boundary layer under the Boussinesq approximation are as follows:

$$\frac{\partial \overline{U}}{\partial t} = f\overline{V} - \frac{\partial(\overline{u'w'})}{\partial z} \tag{1}$$

$$\frac{\partial \overline{V}}{\partial t} = -f\overline{U} - \frac{\partial(\overline{v'w'})}{\partial z} \tag{2}$$

$$\frac{\partial \overline{\theta}}{\partial t} = \frac{1}{\rho_0 c_p}\frac{\partial I}{\partial z} - \frac{\partial(\overline{\theta'w'})}{\partial z} \tag{3}$$

$$\frac{\partial \overline{S}}{\partial t} = -\frac{\partial(\overline{s'w'})}{\partial z} \tag{4}$$

$$\frac{\partial \overline{e}}{\partial t} = -\left(\overline{u'w'}\frac{\partial \overline{U}}{\partial z} + \overline{v'w'}\frac{\partial \overline{V}}{\partial z}\right) + \overline{b'w'} - \frac{\partial}{\partial z}\left(\overline{ew'} + \frac{1}{\rho_0}\overline{P'w'}\right) - \varepsilon. \tag{5}$$

In the above system $\overline{U}$ and $\overline{V}$ refer to the mean horizontal velocity components in the x and y directions respectively, $\overline{\theta}$ is the mean potential temperature, and $\overline{S}$ is the mean salinity. The mean TKE, $\overline{e} = (\overline{u'^2} + \overline{v'^2} + \overline{w'^2})/2 = q^2/2$, is the only turbulent quantity treated prognostically. The various terms appearing on the right-hand side of the TKE equation are due to shear, buoyancy, transport, and viscous dissipation respectively. The term $(1/\rho_0 c_p)\partial I/\partial z$ in Eq. (3) represents a nonturbulent source flux due to penetrating solar radiation. Labeling the vertical coordinate is z, which is taken to be zero at the ocean surface and pointing upward, t is the time coordinate, and f is the local Coriolis parameter. The reference fluid density is denoted by ρ_0 and the heat capacity at constant pressure is c_p. Primed quantities represent deviations from the mean with $\overline{u'w'}$, $\overline{v'w'}$, $\overline{\theta'w'}$, $\overline{s'w'}$, $\overline{b'w'}$, $\overline{ew'}$, and $\overline{P'w'}$ denoting the turbulent fluxes that must be specified in order to close the system.

We propose to obtain these turbulent fluxes diagnostically through the following relations and include a more detailed discussion of these expressions in the appendix:

$$\overline{u'w'} = -K_m\frac{\partial \overline{U}}{\partial z}, \qquad \overline{v'w'} = -K_m\frac{\partial \overline{V}}{\partial z}, \qquad K_m = S_m l q \tag{6}$$

$$\overline{b'w'} = g(\alpha\overline{\theta'w'} - \beta\overline{s'w'}) \tag{7}$$

$$\overline{\theta'w'} = -K_h\frac{\partial \overline{\theta}}{\partial z} - 0.4w_*\tau_t\frac{\partial(\overline{\theta'w'})}{\partial z} + \frac{1}{2}\alpha g\tau_t\overline{\theta'^2}, \qquad K_h = \tau_t\overline{w'^2} \tag{8}$$

$$\overline{s'w'} = -K_s\frac{\partial \overline{S}}{\partial z} + 0.4\tau_t\left(\frac{w_*\gamma}{h}\overline{s'w'}_0\right), \qquad K_s = K_h \tag{9}$$

$$\overline{ew'} + \frac{1}{\rho_0}\overline{P'w'} = -c_1\frac{q^2}{\varepsilon}\left(\overline{w'^2}\frac{\partial \overline{e}}{\partial z} - 0.2w_*\overline{b'w'}\right) \tag{10}$$

$$\overline{\theta'^2} = -c_2\frac{l}{q}\left(\overline{\theta'w'}\frac{\partial \overline{\theta}}{\partial z} + \theta_*\frac{\partial(\overline{\theta'w'})}{\partial z}\right) \tag{11}$$

$$\overline{w'^2} = \frac{1}{4}q^2 + \frac{B}{4}\frac{l}{q}\overline{b'w'}. \tag{12}$$

While momentum fluxes are assumed to be downgradient, the other turbulent fluxes allow for nonlocal and countergradient contributions. Here K_m, K_h, and K_s represent the eddy viscosities for momentum, heat, and salt respectively; S_m is the momentum viscosity coefficient, g the acceleration due to gravity; α, β the thermal ex-

TABLE 1. List of constants.

Symbol	Description	Value
S_m	Eddy viscosity constant	0.39
B	TKE dissipation constant	16.6
γ	Entrainment parameter	1.2
c_1	Turbulence constant	0.19
c_2	Temperature variance dissipation constant	7.8
c_3	Timescale constant	1.56
α_1	TKE boundary condition parameter	3.25
α_2	TKE boundary condition parameter	3.25
k	von Kármán constant	0.4
c_p	Specific heat of seawater	4,100 J kg^{-1} K^{-1}
z_0	Minimum turbulent length scale	0.0001 m
Pr	Turbulent Prandtl number	1.0
f	Coriolis parameter	$f = 2\Omega \sin\lambda$
g	Acceleration due to gravity	9.81 m s^{-2}
α	Thermal expansion coefficient	0.00025 K^{-1}
β	Haline contraction coefficient	0.00077 ppt^{-1}
ρ_0	Reference seawater density	1,025 kg m^{-3}
ρ_a	Surface air density	1.25 kg m^{-3}

pansion and haline contraction coefficients respectively; h the boundary-layer depth; τ_t the turbulent timescale, l the turbulent length scale; and w_*, θ_* the convective velocity and temperature scales respectively. Lastly, the subscript 0 refers to evaluation at the surface $z = 0$. The thermal expansion and haline contraction coefficients were taken to vary according to the simplified equation of state of Friedrich and Levitus (1972), and the dissipation of TKE is expressed according to Kolmogorov (1942):

$$\varepsilon = \frac{q^3}{Bl}.$$

The values used for the various parameters and constants appearing in the above are listed in Table 1.

A weakness in turbulence closure schemes involves the prescription of the length scale l. Methods of specifying this range from the Blackadar (1962) formula to a prognostic equation for a variable that includes l such as the quantity $q^2 l$ as suggested by Mellor and Yamada (1982) and Mellor (1989) or the dissipation ε as used by Kundu (1980). The difficulty associated with a prognostic equation for the master length scale lies in the lack of reliable closure assumptions for the various terms in the equation. Another way of quantifying the length scale is to introduce different length scales for mixing and dissipation. Such an approach was implemented by Therry and Lacarrère (1983), Bougeault and Laccarère (1989) and Gaspar et al. (1990). In the present model the adopted length scale is the widely used Blackadar formula

$$l = \frac{k(|z| + z_0)}{1 + k|z|/l_0}$$

with

$$\frac{1}{l_0} = \frac{1}{l_{\rm MY}} + \frac{1}{l_b}$$

for locally stable conditions and $l_0 = l_{\rm MY}$ for locally unstable conditions. Here $l_{\rm MY}$ is the Mellor–Yamada asymptotic length scale given by

$$l_{\rm MY} = 0.2 \int_{-\infty}^{0} q|z|\, dz \Big/ \int_{-\infty}^{0} q\, dz,$$

and l_b is the buoyancy length scale

$$l_b = \frac{\sqrt{\overline{e}}}{N}$$

imposed by the underlying stable stratification having a Brunt–Väisälä frequency N, where

$$N^2 = -\frac{g}{\rho_0}\frac{\partial \overline{\rho}}{\partial z} = g\left(\alpha\frac{\partial \overline{\theta}}{\partial z} - \beta\frac{\partial \overline{S}}{\partial z}\right).$$

Near the surface l reduces to the usual ''law-of-the-wall'' behavior and then approaches the value l_0. Below the mixed layer l decreases abruptly due to the thermocline and approaches l_b. The parameter z_0 is used to limit the minimum length scale associated with turbulence near the surface. Later we will discuss how this parameter can be modified to incorporate the effects of wave breaking. The quantity k denotes the von Kármán constant. From the length scale, the timescale is easily obtained through

$$\tau_t = \frac{c_3 l}{q}.$$

Since the velocity scale and salinity flux involves the boundary layer depth h, it is necessary to provide a means of computing this. We view this quantity as a measure of the depth to which a significant level of turbulence penetrates to and believe that this typically corresponds to the boundary layer depth itself. In the literature one encounters several ways of defining this depth; some commonly used methods for determining h include:

1) a bulk Richardson number, Ri_B, criterion;
2) a jump in a quantity (such as temperature or salinity) across the mixed layer; and
3) the extinction of TKE at the base of the mixed layer.

The bulk Richardson number criterion constitutes a traditional approach in estimating h. It is usually defined as

$$\mathrm{Ri}_B = \frac{g[\alpha(\overline{\theta}(z_s) - \overline{\theta}(h)) - \beta(\overline{S}(z_s) - \overline{S}(h))](h - z_s)}{(\overline{U}(z_s) - \overline{U}(h))^2 + (\overline{V}(z_s) - \overline{V}(h))^2}$$

and corresponds to the Richardson number between a near-surface level $z = z_s$ and the boundary-layer bottom $z = h$. Typically, h is taken to occur at the minimum depth at which Ri_B assumes a critical value (usually in the range $0.25 < \mathrm{Ri}_B < 1$). In cases of free convection

with little or no mean shear, this condition can lead to problems since the bulk Richardson number will be large at all depths. Large et al. (1994) introduce a similarity-based modification to the definition of Ri_B that prevents this situation by adding a turbulent velocity term in the denominator. Another customary approach in defining h stems from observation, which reveals that the upper ocean is usually thoroughly mixed. Based on this, the boundary layer depth can be defined as the depth at which the temperature changes by ΔT from its surface value. This depth usually coincides with the seasonal thermocline depth (or halocline depth if salinity is used instead of temperature). In fact, this is the criterion used to determine h from observed bathythermographs (BT), which will be presented later with $\Delta T = 0.1$°C. The third criterion listed involves the turbulent kinetic energy. One would expect that immediately below the mixed layer the TKE should decrease rapidly due to the buoyancy jump present at the base. This marks the ''turbucline,'' which can also be used as a surrogate for h as, for example, in the recent work by Kantha and Clayson (1994). After much experimenting with the above methods we have decided to adopt the extinction of TKE approach since the TKE is computed prognostically in this scheme, and it worked consistently well for the various tests, and last, it was least dependent on the grid spacing. Thus, the boundary layer depth is defined as the depth that bounds the region adjacent to the surface in which active turbulence is present. We associate this with the TKE dropping below some low value chosen to be approximately 10^{-6} m^2 s^{-2}. This value is based on the idea that at the base of the mixed layer

$$l \to l_b = \frac{\sqrt{\overline{e}}}{N}.$$

Using $l \approx 0.5$ m and $N \approx 5 \times 10^{-3}$ s^{-1} (see Gargett 1984, 1988) we find that $\overline{e} = O(10^{-6}$ m^2 s$^{-2})$ and in our usage provides an order of magnitude estimate for the TKE at depth h.

The set of equations (1)–(5) is mainly driven by atmospheric forcing at the surface $z = 0$ through flux conditions. Continuity of stress implies

$$\overline{u'w'}_0 = -\frac{\tau_x}{\rho_0}, \qquad \overline{v'w'}_0 = -\frac{\tau_y}{\rho_0}, \tag{13}$$

where $\boldsymbol{\tau} = (\tau_x, \tau_y)$ represents the wind stress. Similarly, the surface heating/cooling condition is

$$\overline{\theta'w'}_0 = -\frac{Q}{\rho_0 c_p}, \tag{14}$$

where Q represents the net nonsolar heat (i.e., the sum of net longwave radiative, sensible, and evaporative heat fluxes) received at the surface and is positive for heating and negative for cooling. The turbulent kinetic energy at the surface can be specified as

$$\overline{e}_0 = \alpha_1 u_*^2 + \alpha_2 w_*^2. \tag{15}$$

Mellor (1989) discusses how this condition is formally equivalent to a zero TKE flux on a rigid surface assuming the ''law-of-the-wall'' holds. This will be revisited later when we discuss how this condition should be modified to include the effects of wave breaking. Here u_* is the friction velocity, which is related to the wind speed and stress through

$$u_*^2 = \frac{\sqrt{\tau_x^2 + \tau_y^2}}{\rho_0} = \frac{\rho_a}{\rho_0} C_D (U_w^2 + V_w^2),$$

with C_D denoting the drag coefficient, ρ_a the density of air, and (U_w, V_w) the wind velocity components. The quantity w_* is known as the convective velocity scale; while u_* is mechanically generated by the wind, w_* is thermally produced mainly by surface cooling. Physically, w_* can be thought of as a sinking velocity associated with a parcel of fluid undergoing unstable surface forcing and is related to the known surface buoyancy flux, $\overline{b'w'}_0$, through

$$w_* = -(\overline{b'w'}_0 |h|)^{1/3}.$$

Later it will be discussed how w_* should be modified to include Langmuir circulations. Also, more explanation and usage of w_* is given in the appendix. The values assumed by the coefficients α_1 and α_2, as discussed in the appendix, are obtained by considering various balances in the limit that the surface is approached. For salinity, the condition to be satisfied is

$$\overline{s'w'}_0 = -\overline{S}(E - P), \tag{16}$$

where $\overline{S}_0$ is the mean surface salinity and E, P are the evaporation and precipitation rates (in m s^{-1}) respectively.

In addition to the atmospheric forcing at the surface, the mixed layer is also forced from below due to interior mixing consisting of the three processes: shear instability, internal wave breaking, and double diffusion. Interior mixing was implemented by enforcing the eddy viscosities not to fall below specified background values implied by such mixing processes. These processes were parameterized according to Large et al. (1994) and are fully described in their paper.

3. Model performance

The set of parabolic-type evolution equations (1)–(5) were numerically integrated in time using a semi-implicit procedure. To allow for accurate differencing, computations were carried out on a staggered grid, whereby the turbulent fluxes and TKE were computed midway between the grid points for the mean quantities $\overline{U}$, $\overline{V}$, $\overline{\theta}$, and $\overline{S}$. The prognostic variables were treated implicitly to increase numerical stability. At each time step the surface fluxes are known and specified through Eqs. (13)–(16). Using this, the turbulent fluxes beneath the surface were then numerically computed by simultaneously solving the system of equations (6)–(12). Oth-

er quantities such as h, τ_t, K_m, K_h, and K_s were computed explicitly based on information from the previous time step since these quantities vary more slowly with time. This also accelerates the convergence of the numerical scheme. Typical computational parameters used were $\Delta t = 500$ s, $\Delta z = 2$ m, and a bottom located at $z = -150$ m.

The model described in the previous section was first subjected to a selected set of tests with idealized forcings including wind-deepening, heating, and cooling cases. The test cases chosen have been considered by others. This provides a direct comparison of the present model against existing mixed layer models, which span from bulk to turbulence closure schemes and also include the well-cited Pollard et al. (1973, hereafter PRT) model as well as the recent K profile parameterization (KPP) model of Large et al. (1994). For comparison purposes, the mixed layer depth was one selected quantity since it is well documented in the literature and in many cases represents the only quantity available. A more appropriate comparison would be based on profiles that we have also included. In an attempt to make a proper comparison, computational parameters similar to those utilized by the authors were used.

We do, however, encounter an uncertainty associated with the definition of the mixed layer depth. Observations compute this depth based on a ΔT criterion, while most mixed layer models are designed to operate with a Ri_B criterion. In most of the cases to be presented (with the exception of the heating experiment) all of these definitions, including the TKE extinction method, produce depths that are sufficiently close to each other in magnitude, thus suggesting little practical distinction between these methods. Also, we will see that the TKE extinction method agrees reasonably well with observational data that cover a wide selection of forcing scenarios. There may be conceivable situations in which the mixed layer undergoes rapid shallowing due to rapid reductions in the surface wind stress or an increase in surface heating. Features of the associated dynamical response, such as inertial oscillations, may give rise to local shear zones that are favorable sites for generation of turbulence and internal mixing. We believe that the model is able to reproduce this shallowing process and damping of inertial oscillations by internal mixing processes that, as noted above, are represented following Large et al. (1994).

a. Wind deepening

The first wind-driven case considered is that conducted by Martin (1985, 1986) where comparisons have been made with the Mellor–Yamada level 2 (1974), level 2.5 (1982), and Therry-Lacarrère (1983) turbulence closure schemes, as well as with the Niiler (1975), Garwood (1977), and Price–Weller–Pinkel (1986) bulk models. For this experiment the initial stratification was 0.05° C m^{-1}, the salinity was constant at 35 psu, the surface heat and salinity fluxes were zero, and the inertial period was 24 h. Displayed in Table 2 are boundary and mixed layer depths after 5 days of forcing for wind stress values of 1, 4, and 16 dyn cm^{-2} (1 dyn cm^{-2} = 0.1 N m^{-2}) acting on an initially shearless and motionless fluid having $\overline{U}(z, t = 0) = \overline{V}(z, t = 0) = 0$. As expected, the final depths are proportional to the square root of the wind stress. Perhaps surprisingly, under this forcing the present model appears to behave more like the Garwood and Niiler bulk models than like the Mellor–Yamada models. The reason for this lies in the stability functions utilized in those schemes. For example, in the level 2.5 scheme S_m and S_h, the eddy viscosity coefficients for momentum and heat respectively, can be determined algebraically through (Mellor 1989):

$$S_h[1 - (3A_2B_2 + 18A_1A_2)G_H] = A_2(1 - 6A_1/B_1)$$

$$S_m(1 - 9A_1A_2G_H) - S_h[(18A_1^2 + 9A_1A_2)G_H] = A_1(1 - 3C_1 - 6A_1/B_1),$$

where

$$G_H = \left(\frac{l^2}{q^2}\right)\left(\frac{g}{\rho_0}\right)\frac{\partial \rho}{\partial z},$$

and $(A_1, A_2, B_1, B_2, C_1) = (0.92, 0.74, 16.6, 10.1, 0.08)$. These expressions result from the closure approximations that they have made and do not apply to our formulation. As a curiosity, we imposed these constraints on S_m and S_h and found that our results came in close agreement with theirs.

TABLE 2. Comparison of boundary and mixed layer depth (in meters) with various models for the wind-deepening case.

	Wind stress (dyn cm^{-2})		
	1	4	16
Mellor–Yamada level 2	19	41	76
Mellor–Yamada level 2.5	18	39	76
Niiler	27	54	108
Garwood	26	51	104
Price–Weller–Pinkel	20	44	88
Therry–Lacarrère	22	46	87
Present model	23	50	107

The next case considered corresponds to a steady wind stress of 0.3 N m^{-2}, constant temperature gradient of 0.1° C m^{-1} and initial velocity profiles $\overline{U}(z, t = 0) = \overline{V}(z, t = 0) = 0$ as used in the work by Pollard et al. (1973). Plotted in Fig. 1 is the mixed layer depth according to the PRT model and our boundary layer depth versus time. Time has been made dimensionless by normalizing it with half the inertial period, $T = \pi/f$. The diagram shows that for early times the two models agree well and behave like $h \sim u_* \sqrt{(t/N)}$. This behavior was also confirmed in the work of Kundu (1981) by

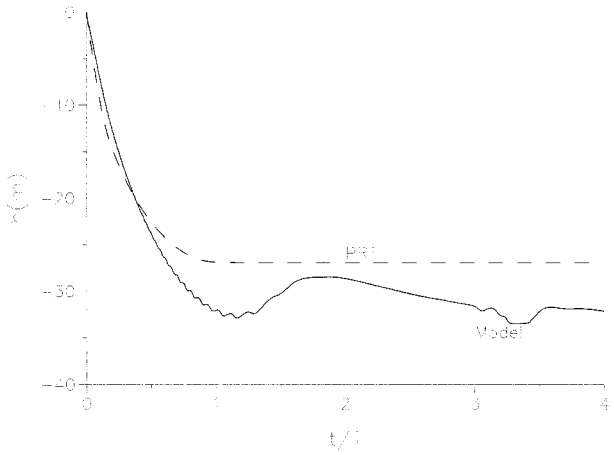

FIG. 1. Comparison of the evolution of h with the PRT model.

assuming a self-similar structure in the flow for early times. After half an inertial period, deepening in the PRT model is arrested by rotation and the mixed layer depth remains constant, while the present model shows a transition occurring in the growth rate. The small oscillations observed are from fluctuations in shear at the base due to mixing, while the larger oscillation is due to inertial motions.

b. Heating

For the heating experiment the model was initialized as in Martin (1985, 1986) with a uniform temperature from the surface down to a depth of 100 m and a linear stable stratification of 0.05° C m^{-1} below and zero initial velocity profiles. Also, it was forced with a constant wind stress of 1 dyn cm^{-2} and heat fluxes of 150, 600, 2400 ly day^{-1} (1 ly day^{-1} = 0.484 W m^{-2}) applied at the surface (with no solar radiation). This case represents the opposing effects of mixing due to wind generated turbulence and the stabilizing effect of surface heating. As in the wind-deepening case, all the turbulent fluxes collapse to downgradient expressions. In Table 3 the boundary layer depth of the present model is contrasted with the mixed layer depths of several models after 2 days of forcing. Our model behaves closest to the models of Mellor–Yamada for this stable case. For stronger heating all the differential models behave similarly. The Niiler and Garwood bulk models produce shallow mixed layer depths for the heating experiment. It was observed that our model produced significant stratification near the surface for high surface heat fluxes indicating that mixing was not strong enough to keep the mixed layer temperature uniform. This is to be expected though since the source of heat is at the surface with no penetration into the fluid column, as would be the case if solar radiation were present. As commented in Martin (1986), this also occurred with the other turbulence closure schemes; the bulk models, on the other hand, respond quickly and hence display little stratification. The heating case produces an example of the difficulties that arose in using the Ri_B and ΔT criteria for determining h. Because of the large stratification that can occur near the surface, these two criteria predicted an unrealistically shallow depth for high heating rates, whereas the TKE criterion was not so affected by the presence of such a stratification. One must bear in mind though that this heating experiment is unrealistic since high heating rates are expected to occur as a result of solar radiation and hence allowed to decay beneath the surface. This was not the case in this experiment.

TABLE 3. Comparison of boundary and mixed layer depth (in meters) with various models for the heating case.

	Surface heat flux (ly/day)		
	150	600	2400
Mellor–Yamada level 2	28	16	8
Mellor–Yamada level 2.5	28	16	8
Niiler	17	4	1
Garwood	33	14	4
Price–Weller–Pinkel	36	18	10
Therry–Lacarrère	38	20	10
Present model	30	19	10

c. Cooling

We begin examination of the effects of convection by simulating the case considered by Martin (1985, 1986). Here, the initial conditions were identical to those in the wind-deepening case. Forcing is due to a constant wind stress of 1 dyn cm^{-2} and surface fluxes of −100, −200, and −300 ly day^{-1}. Table 4 compares the boundary and mixed layer depths of several models after a forcing duration of 120 days. The long forcing period simulates the cooling typical of the winter season and also magnifies the differences in the various models. The shallowest mixed layer depths result from the Mellor–Yamada, Price–Weller–Pinkel, and Therry–Lacarrère models, while the deepest from the Niiler model. The further deepening beyond the shallowest depths in the present model can be attributed to the nonlocal and countergradient contributions to the turbulent fluxes, which are activated in convective situations. Plotted in

TABLE 4. Comparison of boundary and mixed layer depth (in meters) with various models for the cooling case.

	Surface heat flux (ly/day)		
	−100	−200	−300
Mellor–Yamada level 2	72	105	122
Mellor–Yamada level 2.5	72	104	122
Niiler	101	127	150
Garwood	90	117	140
Price–Weller–Pinkel	71	102	126
Therry–Lacarrère	76	104	126
Present model	76	109	133

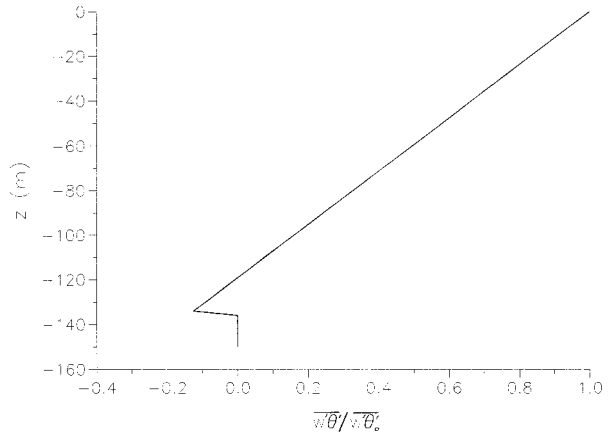

FIG. 2. Normalized heat flux profile after 120 days of cooling at $Q = -300$ ly day^{-1} and a wind stress of 1 dyn cm^{-2}.

Fig. 2 is the normalized heat flux profile at the end of the 120 day run for the cooling rate of -300 ly day^{-1}. The diagram reveals that the magnitude of the flux generated at the base of the mixed layer is about 15% of the surface value, which is consistent with observational findings on convective boundary layers (Stull 1976).

The next comparisons are for the important case of free convection. Listed in Table 5 are the boundary layer depths for the experiment proposed by Large et al. using their similarity-based KPP model. The surface is subject to a steady cooling of -100 W m^{-2} and has an initial linear stable stratification of 0.1° C m^{-1}. As with all these idealized forcing examples, the salinity was kept constant. The depth shown is after 3 days of cooling and are in good agreement. Also presented in Table 6 are boundary layer depths at various times for a case conducted with the third-order model of André–Lacarrère. The agreement for this experiment is within 11%. Here, the surface is cooled at -200 W m^{-2} and the initial profiles as well as the profiles at later times are illustrated in Figs. 3a and 3b. Also shown in these diagrams are the corresponding results of André–Lacarrère, which are represented as dots. The agreement demonstrates that our second-order model does reasonably well in reproducing their velocity and temperature structures. In Fig. 3a we see that convectively generated turbulence is capable of efficiently mixing momentum throughout the mixed layer in contrast to wind generated turbulence, which typically produces an almost constant shear throughout the mixed layer. Also, the temperature profiles in Fig. 3b remain slightly unstable near the surface due to the cooling.

d. Ocean weather station datasets

In addition to the above simple forcing experiments, the model was further tested against observational data taken from Ocean Weather Stations (OWS) November (N) and Papa (P) located in the North Pacific at 30°N, 140°W and 50°N, 145°W respectively. For these simulations the model was run with a uniform 5-m grid spacing that extended down to a depth of 200 m and a 15-min time step. The sensitivity of the results to the grid spacing will be briefly discussed later in this section. Since previous studies such as Martin (1985, 1986), Large et al. (1994), and Kantha and Clayson (1994) have focused on the year 1961, we have decided to follow suit and begin our simulations on 1 January, which we denote as day 0. The datasets consist of 3-h meteorological and BT observations that were used to initialize the temperature profiles. Unfortunately, no velocity, salinity, or TKE measurements are available. This, of course, raises the concern of how to initialize these profiles as well as the sensitivity to these unknown profiles. These sensitivity issues will be addressed later when we present the results for OWS P. From the meteorological data (which included SST, air, wet-bulb, and dewpoint temperatures, wind speed and direction, cloud cover, and surface air pressure) surface fluxes of heat, momentum, evaporation, and radiation can be computed. To do this we utilized the bulk formulas that are fully described in Martin (1985). Fluxes required by the model between the 3-h measurements were obtained by interpolation. As previously mentioned, the boundary layer depth can be determined from the observed BT using a temperature jump criterion. It was defined as the depth at which the temperature drops by 0.1°C from the sea surface value. The effects of advection were not taken into account in our simulation, and the consequences of this will be commented on later. The extinction of solar radiation in seawater as classified by Jerlov (1976) according to turbidity was used in the model with optical type I at OWS N and type II at OWS P. Last, we have assumed a 6% surface albedo at both stations.

At OWS N salinity was held constant during the yearlong simulation. The justification for ignoring salinity effects is supported by the 20 years of analysis of meteorological and oceanographic data performed by Dorman et al. (1974). Also, the velocity and TKE profiles

TABLE 5. Comparison of boundary layer depth (in meters) with the KPP model for the case of free convection for surface heat flux = -100 W m^{-2}.

KPP model	13.6
Present model	12.8

TABLE 6. Comparison of boundary layer depth (in meters) with the third-order model of André and Lacarrère for the case of free convection.

André–Lacarrère model	Present model	Time (hours)
8.0	7.8	5
10.5	9.3	10
12.5	11.1	15

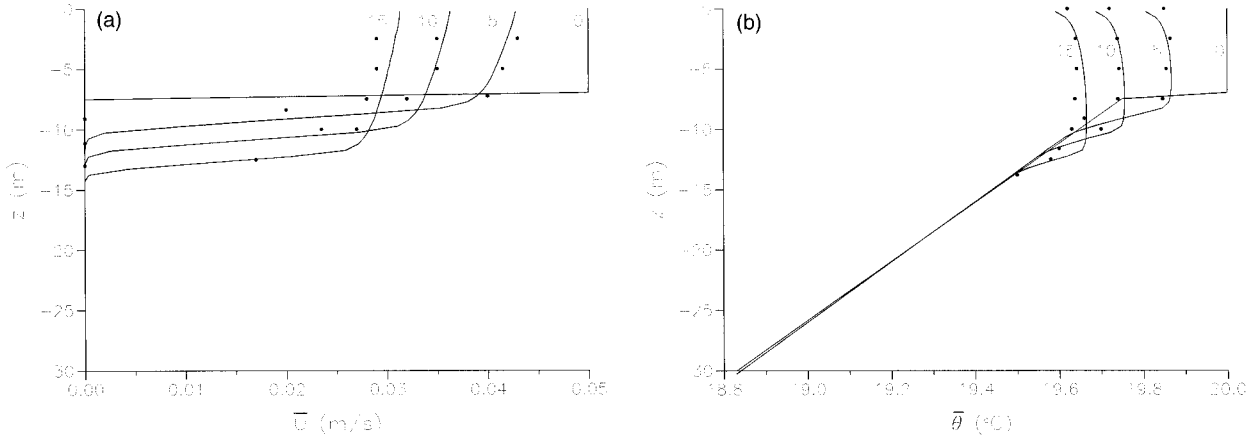

FIG. 3. Profiles of (a) $\overline{U}$ and (b) $\overline{\theta}$ at various times for a free convection experiment with a steady cooling of $Q = -200$ W m^{-2}. The dots reflect corresponding values obtained by the third-order model of André–Lacarrère.

were initially set to zero. The clear-sky insolation was corrected for cloud cover using the correction and solar transmission coefficient set forth by Reed (1977). The results of the simulation are shown in Figs. 4a–c. Obvious features of the simulated SST are spikes that occur during the spring and summer. Similar spikes are also present in the models used by Martin (1985, 1986) and that of Kantha and Clayson (1994) and are the result of the combination of strong heating and weak winds acting on a shallow mixed layer. Figures 4a and 4b contrast the observed and simulated SST and boundary layer depth respectively. Large differences in the SST are apparent in Fig. 4c. However, as explained in Martin (1985), the observed SST at OWS N does show some spurious features where the temperature jumps abruptly and should be taken into account when evaluating the comparison.

For simulations carried out at OWS P the clear-sky insolation was corrected for cloud cover using the correction and solar transmission coefficient of Tabata (1964). Salinity must be treated more carefully since the works of Beatty (1977) and Tabata (1965) both report that a strong halocline exists below a depth of ~125 m. The climatological data of Beatty was used to initialize the salinity profile. To investigate the sensitivity to salinity effects we ran several simulations. First, we ran a trial simulation having a constant initial salinity profile (instead of the climatological data of Beatty), which of course ignored the halocline. In the second simulation we set the salinity flux to zero during the entire run, as did Martin, and used the climatological data for the initial salinity profile. For the third simulation we followed the suggestion of Gaspar (1988), which is to keep the initial salinity profile constant throughout the entire year (again using the profile of Beatty). Last, a fourth simulation was performed similar to the second with the exception that the salinity flux was not set to zero but estimated based upon evaporation that was computed and precipitation that was specified according to the observed mean annual cycle of Tabata (1965). For the three simulations, excluding the first case, the resulting SST profiles were only slightly different from one another and thus justifies using the climatological data as a reasonable initial salinity profile. As to be expected, ignoring the halocline produced a significantly deeper mixed layer during the wintertime.

To investigate the sensitivity to the initial velocity profiles we again ran several simulations whereby different initial profiles were selected ranging from the trivial choice $\overline{U}(z, t = 0) = \overline{V}(z, t = 0) = 0$ to various linear profiles. The results showed negligible dependence on the initial velocity profiles. The velocity profiles after a short time, on the order of days, were virtually independent of the initial profiles. Last, the sensitivity to the initial TKE profile was also studied. Here we considered two initial profiles: the trivial choice $\overline{e}(z, t = 0) = 0$ and expression (A8) derived in the appendix. Once again the results revealed negligible dependence on the initial TKE profile. Presented and contrasted in Figs. 5a–c are observed and simulated SST and boundary layer depth profiles for the case where evaporation and precipitation were incorporated. The agreement between the observed and simulated SST, as shown in Fig. 5a, is good as is the agreement in h portrayed in Fig. 5b. Figure 5c reveals that noticeable discrepancies occur in the final and summertime SST where in both instances the model overestimates the observed value. The final SST is overestimated by about 0.9°C. A similar overestimation was also obtained by Kantha and Clayson and as they mention could be partly attributed to the neglect of advection effects. Large et al. (1994) point out that horizontal advection is important during the period running from September to February. Another apparent difference is an underpredicted mixed layer depth during the winter due to the strong halocline. Since the observed depth is based solely on temperature, it mimics the thermocline depth and does not take into account the halocline. Plotted in Fig. 6 are simulated

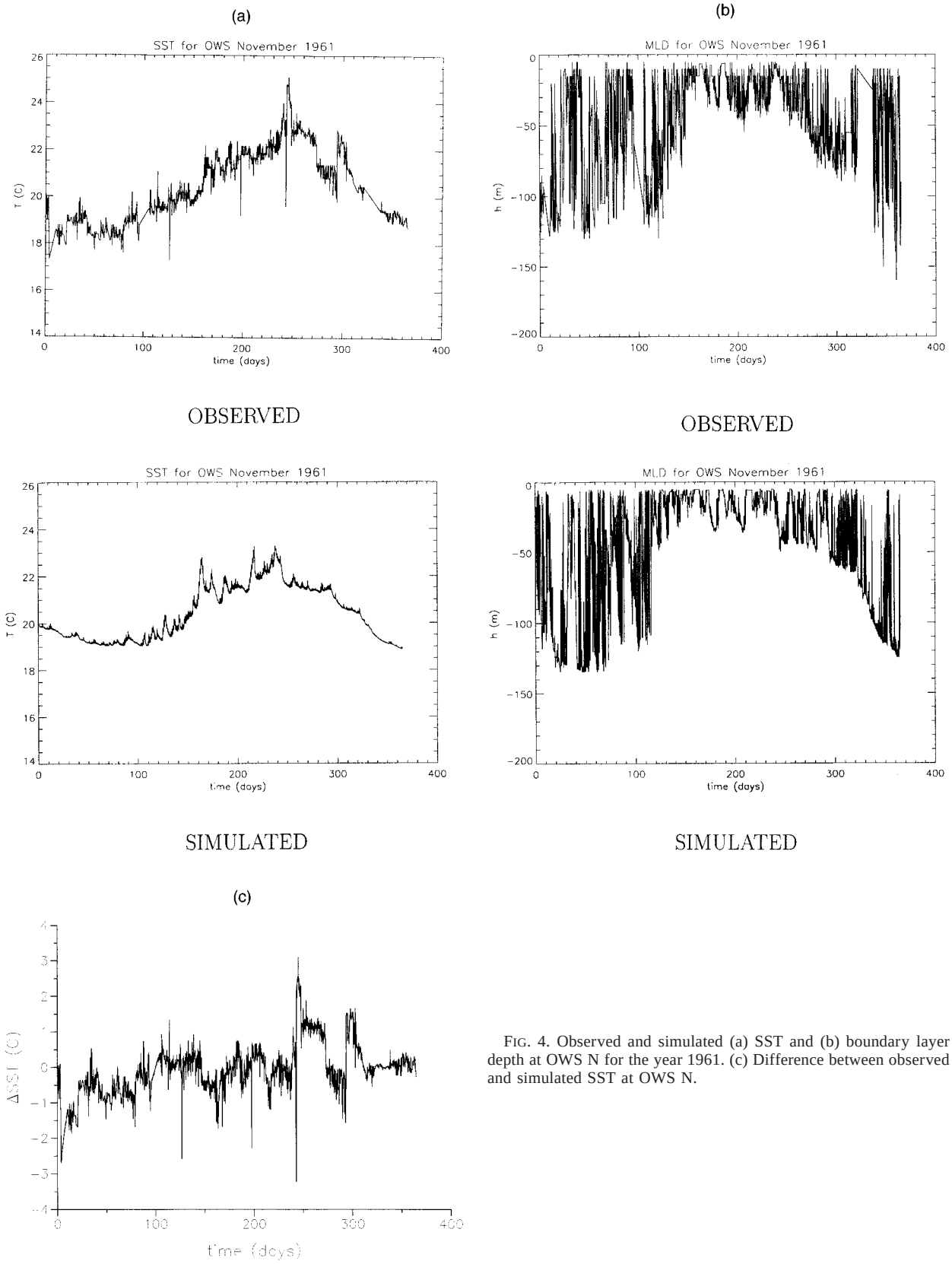

FIG. 4. Observed and simulated (a) SST and (b) boundary layer depth at OWS N for the year 1961. (c) Difference between observed and simulated SST at OWS N.

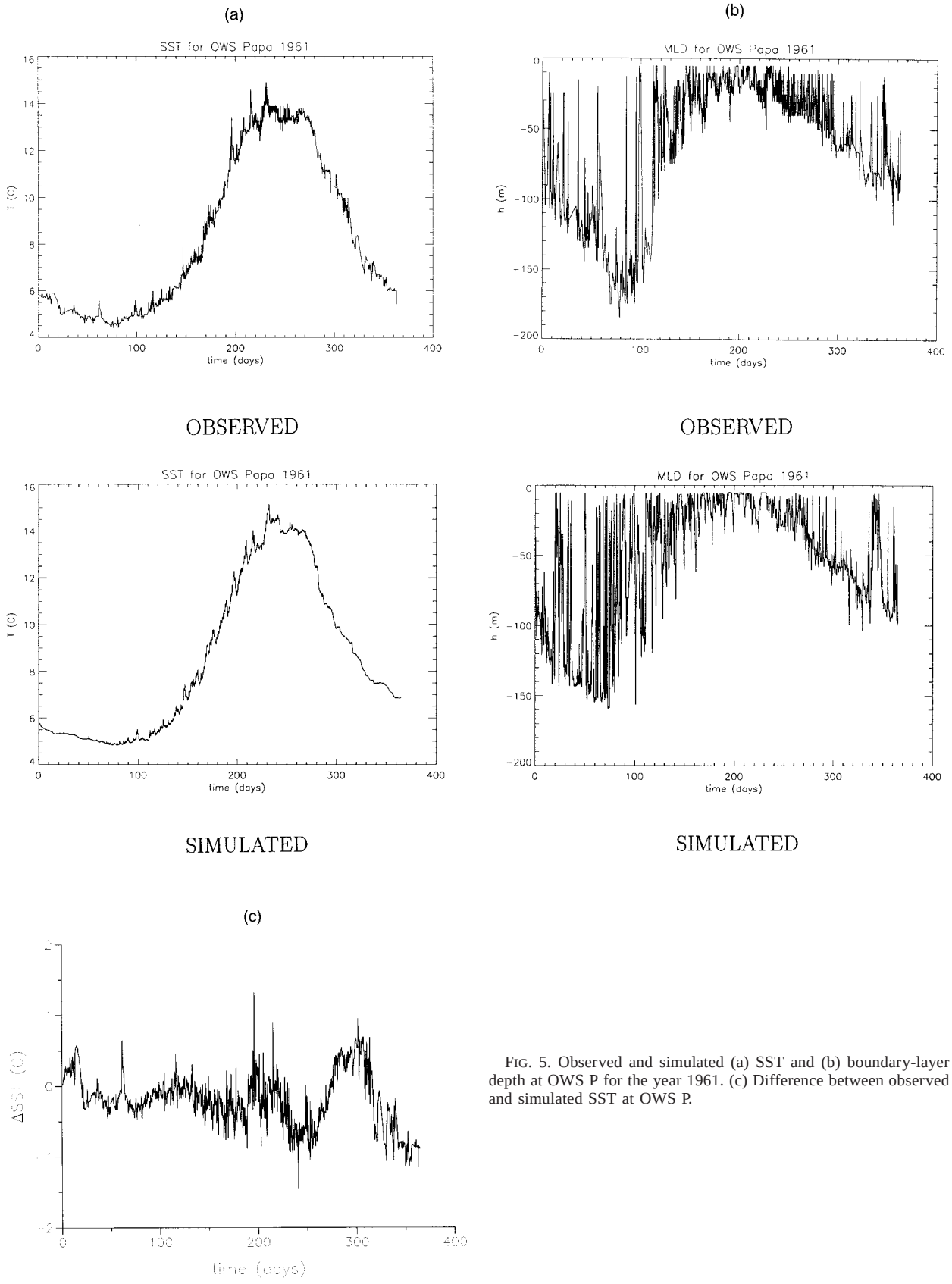

FIG. 5. Observed and simulated (a) SST and (b) boundary-layer depth at OWS P for the year 1961. (c) Difference between observed and simulated SST at OWS P.

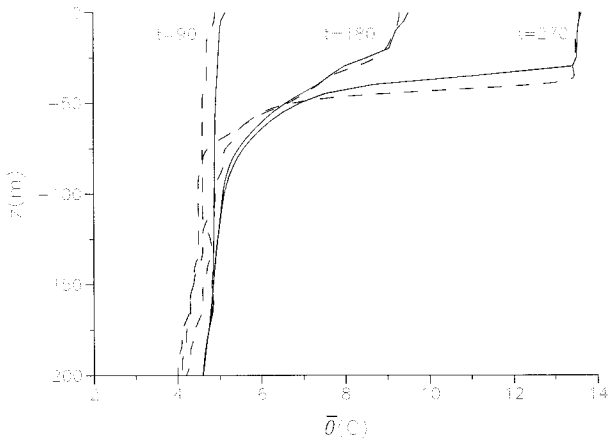

FIG. 6. Comparison of simulated (solid line) and observed (dashed line) temperature profiles for OWS P at $t = 90$, 180, and 270 days.

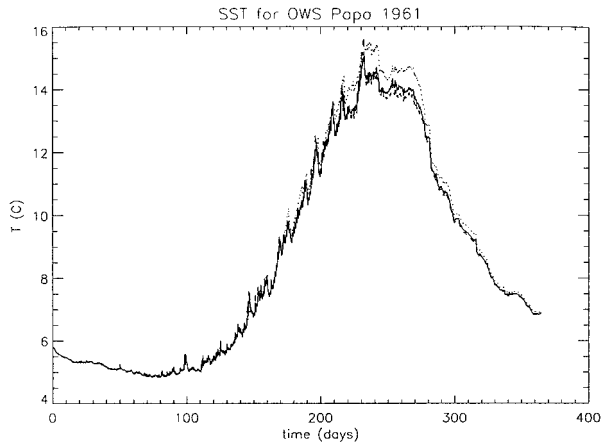

FIG. 7. Simulated SST at OWS P using three grid spacings: $\Delta z = 2.5$ m (dashed line), $\Delta z = 5$ m (solid line), and $\Delta z = 10$ m (dotted line).

and observed temperature profiles at various times during the year-long simulation. This illustrates that the model is able to reasonably capture the seasonal temperature structure in addition to the seasonal SST. We also carried out experiments where the grid spacing was varied. Illustrated in Fig. 7 are the SST profiles corresponding to the three resolutions: $\Delta z = 2.5$ m, $\Delta z = 5$ m, and $\Delta z = 10$ m. The three profiles are in good agreement and show the largest difference occurring during the summertime. This is to be expected though since the mixed layer can get quite shallow and sensitive to the minimum depth allowed, which was set equal to the grid spacing Δz. As a final note we wish to comment that computing h using the different criteria mentioned (i.e., using Ri_B and ΔT) produced similar profiles for the boundary layer depth as that presented. Since the agreement with the observed depth is reasonable, this supports our approach in using the TKE extinction method.

4. Extensions

The structure of the oceanic surface layer is complicated by the presence of surface gravity waves. A consequence of this is that the oceanic surface layer is subjected to some unique processes having no atmospheric counterpart, such as Langmuir circulation and wave breaking. In this section we will discuss how the present model can be modified to include these effects by treating each process separately and independent of each other.

a. Langmuir circulation

Langmuir circulations can be described as organized convective motions in the surface layer of the ocean that play a prominent role in upper-layer mixing. Apart from surface and internal gravity waves, Langmuir cells are considered to be the most important coherent structures in the ocean boundary layer according to Weller and Price (1988). While numerous theories have been proposed to explain these circulations (see Pollard 1977), the prevailing theory is that due to Craik and Leibovich (1976). This theory claims that Langmuir circulations are an instability arising from the nonlinear interaction between the Stokes drift and the frictional wind drift current that is initiated by a vortex force, which enters into the momentum equations. This model is known as the CL2 instability mechanism. Visible manifestations of Langmuir circulations are streaks (or windrows) formed nearly parallel to the wind caused by a series of subsurface counterrotating vortices that closely resemble convection rolls [although they form regardless of surface heating or cooling, the effects of heating or cooling was numerically investigated by Li and Garrett (1995)]. These circulations normally do not exist in winds less than approximately 3 m s^{-1}. Also, they realign themselves with shifts in the wind direction. The wind drift current has larger velocities in the convergence zones. Langmuir (1938) believed that this is because the water there had been on the surface since it rose from the divergence zone and therefore had been accelerated by the wind for the longest period of time. Langmuir also claimed that the vortices are largely responsible for the formation of the thermocline and the maintenance of mixed layers. These circulations have been successfully modeled by Leibovich (1977), Leibovich and Radhakrishnan (1977), and Li and Garrett (1993) using two-dimensional models. Recently, three-dimensional large-eddy simulations of Langmuir circulations have been performed by Skyllingstad and Denbo (1995) and McWilliams et al. (1997), while a three-dimensional model was advanced by Tandon and Leibovich (1995).

To date, ocean models have not yet included the effects of Langmuir circulation. However, using the Price–Weller–Pinkel bulk model Li et al. (1995) and Li and

Garrett (1997) have recently proposed introducing another criterion, called the Langmuir circulation index LC_n, to determine if deepening should occur. This condition is used in addition to the bulk Richardson number criterion and generally produces a deeper mixed layer. The physics behind this criterion is based upon the Froude number, $\mathrm{Fr} = w_d/(Nh)$, where w_d is the maximum downwelling velocity produced by Langmuir circulations in a homogeneous fluid. Their numerical simulations show that this quantity is constant. In the present scheme we have accounted for the effects of Langmuir circulation through the following modifications to the model when the winds exceed 3 m s^{-1}:

1) Adding to the convective velocity, w_*, a mechanically driven contribution due to Langmuir circulation. Here we exploit the nonlocal versatility of our parameterizations for third moments; and
2) including in the equations the contributions arising from the vortex force responsible for producing Langmuir circulations. As we will see this modifies the TKE and momentum equations.

An obvious choice for the mechanical contribution to the convective velocity $w_{*\mathrm{LC}}$ is to use the maximum downwelling velocity w_d. With $|w_d| \approx (0.0025 \text{ to } 0.0085)\sqrt{(U_w^2 + V_w^2}$ (Leibovich 1983) we can write

$$w_{*\mathrm{LC}} \approx -c\sqrt{(U_w^2 + V_w^2)},$$

where c lies in the range $0.0025 < c < 0.0085$. The vortex force that must be included in the momentum equations is given by $\mathbf{V}_s \times \boldsymbol{\omega}$ (Leibovich 1977), where $\mathbf{V}_s$ is the Stokes drift velocity and $\boldsymbol{\omega}$ is the absolute vorticity. The Stokes drift can be parameterized as in Li and Garrett (1993) for a fully developed sea:

$$\mathbf{V}_s = (U_s, V_s) \approx 0.016 \exp(-|z|/L)(U_w, V_w)$$

with

$$L = 0.12(U_w^2 + V_w^2)/g.$$

Owing to the assumption of horizontal homogeneity, adding the vortex force to the momentum equations only affects the Coriolis terms. This has been pointed out in the very recent work of McWilliams et al. (1997). The Coriolis terms in Eqs. (1) and (2) become $f(\overline{V} + V_s)$ and $-f(\overline{U} + U_s)$, respectively, which now include the Stokes drift. Another consequence of adding the vortex force to the momentum equations is a modification to the TKE equation, which now takes the form

$$\frac{\partial \overline{e}}{\partial t} = -\left[\overline{u'w'}\left(\frac{\partial \overline{U}}{\partial z} + \frac{dU_s}{dz}\right) + \overline{v'w'}\left(\frac{\partial \overline{V}}{\partial z} + \frac{dV_s}{dz}\right)\right] + \overline{b'w'} - \frac{\partial}{\partial z}\left(\overline{ew'} + \frac{1}{\rho_0}\overline{P'w'} - U_s\overline{u'w'} - V_s\overline{v'w'}\right) - \frac{q^3}{Bl}. \quad (17)$$

A full derivation of the above is given in the work by Skyllingstad and Denbo (1995). The result is that the following new terms appear on the right-hand side of the TKE equation:

$$U_s\frac{\partial}{\partial z}(\overline{u'w'}), \qquad V_s\frac{\partial}{\partial z}(\overline{v'w'}),$$

which can be rewritten as

$$U_s\frac{\partial}{\partial z}(\overline{u'w'}) = \frac{\partial}{\partial z}(U_s\overline{u'w'}) - \overline{u'w'}\frac{dU_s}{dz}$$

$$V_s\frac{\partial}{\partial z}(\overline{v'w'}) = \frac{\partial}{\partial z}(V_s\overline{u'w'}) - \overline{v'w'}\frac{dV_s}{dz}.$$

Written in this way we see that the shear production and transport terms have been modified by the inclusion of the vortex force. The shear production term (SP) now reads

$$\mathrm{SP} = \left[\overline{u'w'}\left(\frac{\partial \overline{U}}{\partial z} + \frac{dU_s}{dz}\right) + \overline{v'w'}\left(\frac{\partial \overline{V}}{\partial z} + \frac{dV_s}{dz}\right)\right].$$

To investigate the outcome of these modifications we ran the yearlong simulation at OWS P with Langmuir circulation since the winds are stronger there and the dataset is of better quality. The results of that simulation with $c = 0.006$ are illustrated in Figs. 8a,b. In Fig. 8a we plot the boundary layer depth, which shows episodes of dramatic deepening at various instances; illustrated in Fig. 8b is a running 5-day average of the depth difference with and without Langmuir circulation. It is clear from these diagrams that the effects of Langmuir circulation, as implemented here, can lead to further deepening. This deepening is especially prevalent during the fall and winter when convection and winds are stronger. The only noticeable change in the sea surface temperature worth mentioning is a drop in the final SST of about 0.2°C compared to the case with no Langmuir circulation. The inclusion of Langmuir circulation does improve the agreement with observation in that the rms value of the difference between the observed and simulated h is reduced slightly and also the overestimation in SST near the end of the simulation is lowered. As a final note, the modified shear production term suggests redefining the bulk Richardson number Ri_B as follows:

$$\mathrm{Ri}_B = \frac{g[\alpha(\overline{\theta}(z_s) - \overline{\theta}(h)) - \beta(\overline{S}(z_s) - \overline{S}(h))](h - z_s)}{(\overline{U}(z_s) - \overline{U}(h))^2 + (\overline{V}(z_s) - \overline{V}(h))^2 + |\Delta\mathbf{V}_s|^2},$$

where

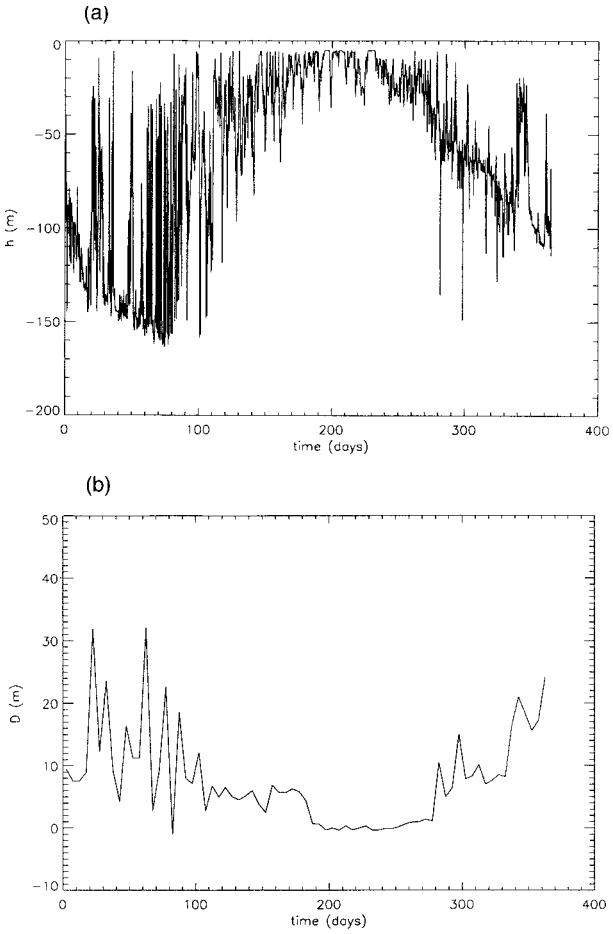

FIG. 8. (a) Simulated boundary layer depth at OWS P with Langmuir circulation. (b) Averaged depth difference D, with and without Langmuir circulation.

$$|\Delta \mathbf{V}_s|^2 = (U_s(z_s) - U_s(h))^2 + (V_s(z_s) - V_s(h))^2.$$

Using the prescribed expressions for the Stokes drift with $h \gg L$ and $z_s \to 0$, we find that

$$|\Delta \mathbf{V}_s|^2 \approx (0.016)^2(U_w^2 + V_w^2) = (0.016)^2\left(\frac{\rho_0}{\rho_a}\right)\frac{u_*^2}{C_D}$$
$$\approx 160u_*^2.$$

It is interesting that the modified expression for Ri_B comes in close agreement with one proposed by Vogelezang and Holtslag (1998), for atmospheric use under stable conditions. Also, Large et al. (1994) suggest a form for Ri_B that is similar to that above whereby they replace $|\Delta \mathbf{V}_s|^2$ with a turbulent velocity. We point out that the above expression for Ri_B was not used in our case since the TKE extinction method was implemented to compute h and we offer the above only as an alternative.

b. Breaking waves

The recent measurements of Drennan et al. (1996), Terray et al. (1996), Anis and Moum (1992), Agrawal et al. (1992), and Gargett (1989), to mention a few, support the idea of enhanced turbulence in the oceanic surface layer as a result of wind wave action. In previous studies, for example Kundu (1980) and Klein and Coantic (1981), wave breaking is taken into account by prescribing a nonzero TKE flux at the surface $z = 0$. Following this approach, as in the recent work of Craig and Banner (1994), we proceed to investigate the consequences of this on the present scheme. This involves examining the limiting behavior of the TKE equation (5) in its steady-state form near the surface. In the absence of a surface buoyancy flux we expect that

$$l \to k(|z| + z_0)$$
$$\mathrm{SP} \to \frac{u_*^4}{K_m}$$
$$\overline{ew'} \to -\alpha_e K_m \frac{\partial \overline{e}}{\partial z}, \qquad \alpha_e = \frac{3B}{64S_m}.$$

The TKE equation then assumes the form of a nonlinear ordinary differential equation given by

$$(1 + \zeta)\frac{d}{d\zeta}\left\{(1 + \zeta)\frac{d(q^3)}{d\zeta}\right\} - n^2q^3 = -n^2\lambda/q, \quad (18)$$

where $\zeta = |z|/z_0$, $n^2 = 3/(Bk^2S_m\alpha_e)$ and $\lambda = Bu_*^4/S_m$. This equation represents a three-way balance between shear, diffusion, and dissipation. In the absence of diffusion we get the familiar shear–dissipation balance given by $q = \lambda^{1/4}$. Craig and Banner also considered the balance between diffusion and dissipation to arrive at the dominant solution

$$q = C'(1 + \zeta)^{-n/3},$$

where C' is an arbitrary constant. Physically, this solution represents the decay in TKE from the surface where it is presumably generated. Our objective here is to present a more general solution to (18) that reduces to the above result when the right-hand side of (18) tends to zero. We begin by making the substitution $(1 + \zeta) = \exp(\xi)$ and cast the equation in dimensionless form by defining $\hat{q} = q/\lambda^{1/4}$ and rescaling ξ as $\hat{\xi} = n\xi$. Then, in terms of $\hat{q}^2$, Eq. (18) can be rewritten as

$$\frac{3}{4}\left(\frac{d(\hat{q}^2)}{d\hat{\xi}}\right)^2 + \frac{3}{2}\hat{q}^2\frac{d^2(\hat{q}^2)}{d\hat{\xi}^2} - (\hat{q}^2)^2 = -1. \quad (19)$$

In this form the shear–dissipation balance becomes simply $\hat{q} = 1$. Next we set $\hat{q}^2 = 1 + F$, where F denotes an enhancement factor above the shear–dissipation value due to wave breaking, and define $R = dF/d\hat{\xi}$ so that $dR/d\hat{\xi} = RdR/dF$. With these in place and after some algebra we obtain

$$R = \frac{dF}{d\hat{\xi}} = -\frac{2}{3}F\sqrt{\frac{3+F}{1+F}}. \quad (20)$$

In arriving at this expression we have invoked the condition that $R = 0$ when $F = 0$ and have chosen the negative root to give the desired asymptotic behavior, which is that $\hat{q}^2 \to 1$ sufficiently far away from the surface. Before presenting the exact solution to (20) we first illustrate two limiting cases:

$$F \gg 3, \quad \text{then } \frac{dF}{d\hat{\xi}} = -\frac{2}{3}F,$$

which recovers the solution of Craig and Banner, and

$$F \ll 1, \quad \text{then } \frac{dF}{d\hat{\xi}} = -\frac{2}{\sqrt{3}}F,$$

which corresponds to the shear–dissipation limit. This demonstrates that, if wave breaking significantly enhances the turbulence, then the balance is established between dissipation and diffusion with little contribution coming from shear. The general solution to (20) is given by

$$\left(\frac{\eta + 2\sqrt{3}}{\eta - 2\sqrt{3}}\right)^{1/\sqrt{3}} = C(\eta + 4)\exp\left(-\frac{2}{3}\hat{\xi}\right), \quad (21)$$

where C is an arbitrary constant and

$$\eta = 2F - 2\sqrt{(3+F)(1+F)}.$$

It can be shown that the solution given by (21) collapses to the limiting forms above when the appropriate limits are taken.

In order to investigate the role of wave breaking we consider the limiting case of large F since in such circumstances wave breaking is expected to be the main source of turbulence. In this case we have $F \to C(1+\zeta)^{-2n/3}$ and $q_2 \to \sqrt{\lambda F}$ in terms of the original variables. If we impose a TKE flux condition as in Kundu (1980) and Klein and Coantic (1981)

$$\overline{ew'}_0 = -mu_*^3,$$

where m is a parameter ranging from about 10 to as high as 100, this enables us to determine the constant C and yields $C = 4m^{2/3}\sqrt{S_m/B}$. Since the near surface structure of the TKE is known, this information can be used to convert the above flux condition into a Dirichlet condition and is equivalent to adding a wave breaking component to the coefficient α_1 in the TKE boundary condition giving

$$\overline{\alpha}_1 = 2m^{2/3} + \alpha_1.$$

This limiting case considered becomes more and more valid as m increases. As well, we redefine z_0 with a Charnock-type formula

$$z_0 = \frac{1,400u_*^2}{g}$$

as discussed in Craig and Banner. As noted in the recent review by Melville (1996), the specification of z_0 is an unresolved issue plaguing turbulence closure modeling. Craig and Banner found that in order to yield reasonable agreement with dissipation measurements much larger values of z_0 in the range 0.1–8 m had to be used. Simulations were run with these modifications and although these changes enhanced the turbulence near the surface, it showed a negligible effect in further deepening the mixed layer. This is also consistent with the findings of Kundu (1980) and Klein and Coantic (1981). The explanation for this, which is consistent with the above analysis, is that deeper beneath the surface the TKE becomes controlled by the mean flow through shear production and not by its surface conditions. Since the effects of wave breaking do not directly enter into the equations for the mean, little change in the TKE occurs at larger depths.

Considerable interest has been directed toward the vertical structure of ε and the prediction of its decay rate since the dissipation is a quantity that can be measured with reasonable confidence. Recent measurements (cited earlier) verified the existence of a wave zone characterized by enhanced dissipation due to wave breaking well in excess of

$$\varepsilon \approx \frac{u_*^3}{kz}$$

as suggested by the classical logarithmic boundary layer over a rigid surface. The dissipation was first estimated to decay as z^{-a} with a in the range 3.0–4.6. However, as discussed in Melville (1996) the recent papers by Terray et al. (1996) and Drennan et al. (1996) both point to a slower z^{-2} decay. The decay rate predicted by the Craig and Banner model is given by $z^{-3.4}$. According to the analysis presented above, our dissipation is found to decay with a power law behavior having an index of -2.2 and thus comes in close agreement with the currently accepted inverse square law.

5. Conclusions

Presented in this paper is a second-order turbulence closure scheme for the oceanic mixed layer. While the scheme is similar in some respects to a Mellor–Yamada level 2.5 scheme, it differs substantially in the treatment of the turbulent fluxes. Here, we have allowed for nonlocal and countergradient contributions to the turbulent fluxes by virtue of our parameterizations for third moments. These contributions become activated in convective cases. The scheme computes the boundary layer depth h on the basis of the level of turbulence. Since the TKE decays rapidly beneath the mixed layer and is computed prognostically, it was found to be a good measure for h for the all cases considered. The performance of the model was compared with other turbulence closure and bulk models as well as with the PRT and KPP models for idealized forcing experiments. Also, the model was tested against observations taken at OWS

November and Papa for the year 1961 and did reasonably well in reproducing the observed sea surface temperature and boundary layer depth.

Also considered in this study were means of incorporating near-surface processes such as Langmuir circulations and wave breaking. Accounting for the effects generated by Langmuir circulations involved modifying the convective velocity scale to include a mechanically driven contribution as well as modifying the TKE and momentum equations to include the Craik–Leibovich (1976) vortex force, all of which can be easily absorbed into the present scheme. The results obtained from these modifications using OWS P data indicate that Langmuir circulation causes further deepening of the mixed layer, especially during the fall and winter seasons. Using the data from the Long-Term Upper Ocean Study (LOTUS), Li et al. (1995) also demonstrate that Langmuir circulations can dominate deepening when the velocity difference across the base of the mixed layer is less than about 1% of the wind speed. The analysis presented on wave breaking represents an extension of the pioneering work conducted by Craig and Banner (1994), which constitutes the most recent and thorough attempt in modeling the effects of wave breaking. Here, wave breaking was accounted for by modifying the surface boundary condition for the TKE and by specifying the limiting length scale near the surface with a Charnock-type relation. Although these changes can greatly enhance the turbulence near the surface, it showed little influence in further deepening the mixed layer. This is consistent with the findings of Kundu (1980) and Klein and Coantic (1981). Last, the decay rate of dissipation predicted by the analysis agrees well with the recent measurements of Terray et al. (1996) and Drennan et al. (1996).

Acknowledgments. S.J.D.D. wishes to acknowledge the Natural Sciences and Engineering Research Council of Canada for financial support in the form of a Visiting Postdoctoral Fellowship. Also, we wish to express our thanks to Paul J. Martin of the Naval Ocean Research and Development Activity for providing us with the OWS data for stations N and P and also for helpful discussions. Last, we thank Greg Flato and two anonymous referees for insightful comments that helped improve the paper.

APPENDIX

Derivation of Turbulent Flux Expressions

The derivation of the flux relations (6)–(12) is outlined below. We begin with the heat budget equation for the turbulent heat flux:

$$\frac{\partial(\overline{\theta' w'})}{\partial t} = -\overline{w'^2}\frac{\partial\overline{\theta}}{\partial z} - \frac{\partial(\overline{\theta' w'^2})}{\partial z} - \frac{1}{\rho_0}\overline{\theta'\frac{\partial P'}{\partial z}} + \overline{b'\theta'}. \quad \text{(A1)}$$

First we assume that the turbulence is quasi-steady. This is valid provided the turbulent timescale is much smaller than the timescale associated with the evolving surface conditions. Following Moeng and Wyngaard (1986), the pressure term is expressed as

$$\frac{1}{\rho_0}\overline{\theta'\frac{\partial P'}{\partial z}} \approx \frac{\overline{\theta' w'}}{\tau_t} + \frac{1}{2}\alpha g\overline{\theta'^2}.$$

This result makes use of Rotta's (1951) ''return to isotropy'' model, which is represented by the first term. Equation (A1) then becomes

$$\overline{\theta' w'} = -K_h\frac{\partial\overline{\theta}}{\partial z} - \tau_t\frac{\partial(\overline{\theta' w'^2})}{\partial z} + \frac{\tau_t}{2}\alpha g\overline{\theta'^2}, \quad \text{(A2)}$$

where the eddy viscosity for heat is defined as $K_h = \tau_t\overline{w'^2}$ and we have made the approximation $\overline{b'\theta'} \approx \alpha g\overline{\theta'^2}$. The next step is to parameterize the third moment according to the recent work of Abdella and McFarlane (1997)

$$\overline{\theta' w'^2} \approx 0.4 w_*\overline{\theta' w'}, \quad \text{(A3)}$$

where w_* is the convective velocity established by surface forcing. It is defined by $w_* = -(\overline{b' w'}_0|h|)^{1/3}$ for unstable cases and zero otherwise, with the subscript referring to evaluation at the surface $z = 0$. With these in place Eq. (A2) then agrees with expression (8). In the absence of radiation (8) can be further simplified by arguing that the heat flux should be an approximately linear function of z throughout the mixed layer. This is supported by Fig. 2 where the normalized heat flux is plotted for one of the cooling cases presented in Table 4. Making this assumption on the transport term avoids numerically solving the ODE while still capturing the importance of transport. Thus, in radiation-free cases we can write

$$\frac{\partial(\overline{\theta' w'^2})}{\partial z} = 0.4 w_*\frac{\partial(\overline{\theta' w'})}{\partial z} \approx -0.4\gamma w_*\frac{\overline{\theta' w'}_0}{h},$$

where γ is a constant in the range $1 \leq \gamma \leq 1.3$ and accounts for the level of entrainment at the base of the mixed layer. We emphasize that we have made use of the linear profile of the heat flux only to make an estimate on the transport term.

The expression for the heat flux requires knowledge of the temperature variance $\overline{\theta'^2}$ as well as the vertical velocity variance $\overline{w'^2}$. To obtain $\overline{\theta'^2}$ we start from its budget equation

$$\frac{\partial(\overline{\theta'^2})}{\partial t} = -2\overline{\theta' w'}\frac{\partial\overline{\theta}}{\partial z} - \frac{\partial(\overline{\theta'^2 w'})}{\partial z} - 2\epsilon_\theta. \quad \text{(A4)}$$

As before, we assume the turbulence is quasi-steady and parameterize the third moment according to Abdella and McFarlane:

$$\overline{\theta'^2 w'} \approx 2.0\theta_*\overline{\theta' w'} \quad \text{with } \theta_* = \frac{\overline{\theta' w'}_0}{w_*}, \quad \text{(A5)}$$

where θ_* is the convective temperature scale. Both the parameterizations for $\overline{\theta'^2 w'}$ and $\overline{\theta' w'^2}$ can be traced back to the convective mass flux concept as explained in Abdella and McFarlane. Next we represent the dissipation term according to Kolmogorov (1942)

$$\epsilon_\theta \approx \frac{q}{c_2 l}\overline{\theta'^2}.$$

With this we arrive at the expression given by (11). The equation satisfied by the vertical velocity variance as given by the André et al. (1978) model is

$$\frac{\partial(\overline{w'^2})}{\partial t} = -\frac{\partial(\overline{w'^3})}{\partial z} + 2\overline{b'w'} - \frac{8}{B}\frac{q}{l}\left(\overline{w'^2} - \frac{1}{3}q^2\right) - \frac{2}{3}\frac{q^3}{Bl}. \quad \text{(A6)}$$

Assuming stationarity and ignoring the transport term yields the expression given by (12).

In the parameterization of the TKE flux (10) we have included a buoyancy contribution as in Therry and Lacarrère (1983) to more effectively describe the diffusion of TKE in convective situations. The salinity flux, $\overline{s'w'}$, can be modeled along the same lines as the heat flux. This, however, would introduce the second moments $\overline{s'\theta'}$ and $\overline{s'^2}$, which in turn can be parameterized in a similar fashion as $\overline{\theta'^2}$. Since the influence of these terms is uncertain and is expected to be small for the cases presented here, we have adopted a simpler representation for $\overline{s'w'}$ given by (9). The origin of the countergradient term follows from arguments made for the heat flux. We add that this term represents a nonlocal contribution to the salinity flux since it is derived from surface forcing conditions. Last, the momentum fluxes used in the model are standard downgradient expressions that closely resemble those used in the Mellor and Yamada (1982) scheme. Parameterizing momentum fluxes is complicated by the presence of pressure forces. Assumptions made in modeling other turbulent fluxes, such as heat and salinity, cannot be easily carried over to momentum since there is very little experimental or observational evidence to support this. The downgradient approximation, which is probably not fully adequate for convective cases, results from its budget equation if we assume the following: the transport term approximately cancels the buoyancy term, the pressure term can be parameterized by the return-to-isotropy formulation and finally the steady-state assumption is valid. In view of this, the parameterization of momentum fluxes is worthy of a more thorough independent investigation.

As a final note we wish to comment on the values of the various constants appearing in Table 1. While some of these constants are purely empirical, others are based on physical arguments. For example, we expect that near the surface

$$K_m \to ku_*(|z| + z_0),$$

and, using a simple shear–dissipation balance, obtain

$$q \to \left(\frac{B}{S_m}\right)^{1/4} u_*.$$

Combining these expressions, it is easy to show that

$$B = \frac{1}{S_m^3}.$$

Thus, once S_m is chosen, this immediately fixes the value of B. The value for S_m corresponds to the neutral value of Mellor and Yamada. The constant α_1 appearing in the surface condition for the TKE was found by applying a simple shear–dissipation balance. This leads to

$$\alpha_1 = \frac{1}{2}\sqrt{\frac{B}{S_m}},$$

which is consistent with Mellor and Yamada, and similarly we find that $\alpha_2 = \alpha_1$. Last, the constant c_3 associated with the timescale was determined by imposing the constraint that under neutral conditions $K_h = K_m/\mathrm{Pr}$, where Pr is the turbulent Prandtl number. This leads to the result $c_3 = 4S_m/\mathrm{Pr}$.

A note on TKE initialization

Here we develop a formula for initializing the TKE needed for the yearlong simulations conducted at OWS N and P. We begin with a version of the TKE equation similar to that used in the Mellor–Yamada level 2 scheme in which a quasi-steady state is assumed and eddy transport terms are ignored:

$$0 = -\left(\overline{u'w'}\frac{\partial \overline{U}}{\partial z} + \overline{v'w'}\frac{\partial \overline{V}}{\partial z}\right) + \overline{b'w'} - \frac{q^3}{Bl}. \quad \text{(A7)}$$

All turbulent fluxes are represented by the downgradient expressions

$$\overline{u'w'} = -K_m\frac{\partial \overline{U}}{\partial z}, \qquad \overline{v'w'} = -K_m\frac{\partial \overline{V}}{\partial z},$$

$$\overline{b'w'} = -\alpha g K_h\frac{\partial \overline{\theta}}{\partial z},$$

with $K_m = K_h = K = S_m l q$, as in a Mellor–Yamada level 2.5 scheme. Then rearranging Eq. (A7) yields

$$\overline{e} = \frac{S_m B l^2}{2}\left[\left(\frac{\partial \overline{U}}{\partial z}\right)^2 + \left(\frac{\partial \overline{V}}{\partial z}\right)^2 - \alpha g\frac{\partial \overline{\theta}}{\partial z}\right]. \quad \text{(A8)}$$

The above relation can be used to furnish an initial TKE profile provided the mean variables are specified and a reasonable estimate for l is used, such as $l \approx 2$ m. It is interesting to note that in terms of the gradient Richardson number, defined as

$$\mathrm{Ri}_G = \frac{N^2}{(\partial \overline{U}/\partial z)^2 + (\partial \overline{V}/\partial z)^2},$$

where

$$N^2 = \alpha g \frac{\partial \overline{\theta}}{\partial z},$$

Eq. (A8) can be written alternatively as

$$\overline{e} = \frac{S_m B l^2}{2} \frac{N^2}{\mathrm{Ri}_G}(1 - \mathrm{Ri}_G). \tag{A9}$$

This provides a relationship between the TKE and Ri_G once appropriate values for l and N are specified.

It is interesting to note that, at the base of the mixed layer where we have assumed that

$$l \to l_b = \frac{\sqrt{\overline{e}}}{N},$$

Eq. (A9) yields a critical value for the gradient Richardson number:

$$(\mathrm{Ri}_G)_{\mathrm{cr}} = \frac{1}{1 + \dfrac{2}{S_m B}} < 1,$$

whose magnitude is approximately 0.76. Retaining the transient term in the left-hand side of Eq. (A7) and repeating the above analysis it is easily shown that for $\mathrm{Ri}_G > (\mathrm{Ri}_G)_{\mathrm{cr}}$ the TKE decays exponentially with time while for $\mathrm{Ri}_G < (\mathrm{Ri}_G)_{\mathrm{cr}}$ the TKE grows exponentially with time.

REFERENCES

Abdella, K., and N. McFarlane, 1997: A new second-order turbulence closure scheme for the planetary boundary layer. *J. Atmos. Sci.*, **54,** 1850–1867.

Agrawal, Y. C., E. A. Terray, M. A. Donelan, P. A. Hwang, A. J. Williams, W. Drennan, K. Kahm, and S. Kitaigorodskii, 1992: Enhanced dissipation of kinetic energy beneath breaking waves. *Nature*, **359,** 219–220.

André, J. C., and P. Lacarrère, 1985: Mean and turbulent structures of the oceanic surface layer as determined from one-dimensional, third-order simulations. *J. Phys. Oceanogr.,* **15,** 121–132.

——, G. DeMoor, P. Lacarrère, G. Therry, and R. du Vachat, 1978: Modelling the 24-hr evolution of the mean and turbulent structures of the planetary boundary layer. *J. Atmos. Sci.,* **35,** 1861–1883.

Anis, A., and J. N. Moum, 1992: The superadiabatic surface layer of the ocean during convection. *J. Phys. Oceanogr.,* **22,** 1221–1227.

Ball, F. K., 1960: Control of inversion height by surface heating. *Quart. J. Roy. Meteor. Soc.,* **86,** 483–494.

Beatty, W. H., 1977: Variability of oceanographic conditions at ocean weather stations in the North Atlantic and North Pacific Oceans. NAVOCEANO Tech. Note 3700-67-77, U.S. Naval Oceanographic Office, Washington, D.C., 100 pp.

Blackadar, A. K., 1962: The vertical distribution of wind and turbulent exchange in a neutral atmosphere. *J. Geophys. Res.,* **67,** 3095–3102.

Bougeault, P., and P. Lacarrère, 1989: Parameterization of orography-induced turbulence in a meso-beta scale model. *Mon. Wea. Rev.*, **117,** 1872–1890.

Craig, P. D., and M. L. Banner, 1994: Modeling wave-enhanced turbulence in the ocean surface layer. *J. Phys. Oceanogr.,* **24,** 2546–2559.

Craik, A. D. D., and S. Leibovich, 1976: A rational model for Langmuir circulations. *J. Fluid Mech.,* **73,** 401–426.

Dorman, C. E., C. A. Paulson, and W. H. Quinn, 1974: An analysis of 20 years of meteorological and oceanographic data from ocean station N. *J. Phys. Oceanogr.,* **4,** 645–653.

Drennan, W. M., M. A. Donelan, E. A. Terray, and K. B. Katsaros, 1996: Oceanic turbulence dissipation measurements in SWADE. *J. Phys. Oceanogr.,* **26,** 808–815.

Friedrich, H., and S. Levitus, 1972: An approximation to the equation of state for seawater, suitable for numerical ocean models. *J. Phys. Oceanogr.,* **2,** 514–517.

Gargett, A. E., 1984: Vertical eddy diffusivity in the ocean interior. *J. Mar. Res.,* **42,** 359–393.

——, 1988: The scaling of turbulence in the presence of stable stratification. *J. Geophys. Res.,* **93,** 5021–5036.

——, 1989: Ocean turbulence. *Ann. Rev. Fluid Mech.,* **21,** 419–451.

Garwood, R. W., 1977: An oceanic mixed-layer model capable of simulating cyclic states. *J. Phys. Oceanogr.,* **7,** 455–471.

Gaspar, P., 1988: Modeling the seasonal cycle of the upper ocean. *J. Phys. Oceanogr.,* **18,** 161–180.

——, Y. Grégoris, and J.-M. Lefevre, 1990: A simple eddy kinetic energy model for simulations of the oceanic vertical mixing: Tests at station Papa and Long-Term Upper Ocean Study site. *J. Geophys. Res.,* **95,** 16 179–16 193.

Jerlov, N. G., 1976: *Marine Optics.* Elsevier, 231 pp.

Kantha, L. H., and C. A. Clayson, 1994: An improved mixed layer model for geophysical applications. *J. Geophys. Res.,* **99,** 25 235–25 266.

Klein, P., and M. Coantic, 1981: A numerical study of turbulent processes in the marine upper layers. *J. Phys. Oceanogr.,* **11,** 849–863.

Kolmogorov, A. N., 1942: The equation of turbulent motion in an incompressible fluid. *Izv. Akad. Nauk. SSSR, Ser. Phys.,* **6,** 56–58.

Kraus, E. B., and J. S. Turner, 1967: A one-dimensional model of the seasonal thermocline. Part II. The general theory and its consequences. *Tellus,* **19,** 98–105.

Kundu, P. K., 1980: A numerical investigation of mixed-layer dynamics. *J. Phys. Oceanogr.,* **10,** 220–236.

——, 1981: Self-similarity in stress-driven entrainment experiments. *J. Geophys. Res.,* **86,** 1979–1988.

Langmuir, I., 1938: Surface motion of water induced by wind. *Science,* **87,** 119–123.

Large, W. G., J. C. McWilliams, and S. C. Doney, 1994: Oceanic vertical mixing: A review and a model with a nonlocal boundary layer parameterization. *Rev. Geophys.,* **32,** 363–403.

Leibovich, S., 1977: On the evolution of the system of wind drift currents and Langmuir circulations in the ocean. Part 1. Theory and averaged current. *J. Fluid Mech.,* **79,** 715–743.

——, 1983: The form and dynamics of Langmuir circulations. *Ann. Rev. Fluid Mech.,* **15,** 391–427.

——, and K. Radhakrishnan, 1977: On the evolution of the system of wind drift currents and Langmuir circulations in the ocean. Part 2. Structure of the Langmuir vortices. *J. Fluid Mech.,* **80,** 481–507.

Li, M., and C. Garrett, 1993: Cell merging and the jet/downwelling ratio in Langmuir circulation. *J. Mar. Res.,* **51,** 737–769.

——, and ——, 1995: Is Langmuir circulation driven by surface waves or cooling? *J. Phys. Oceanogr.,* **25,** 64–76.

——, and ——, 1997: Mixed layer deepening due to Langmuir circulation. *J. Phys. Oceanogr.,* **27,** 121–132.

——, K. Zahariev, and C. Garrett, 1995: Role of Langmuir circulation in the deepening of the ocean surface mixed layer. *Science,* **270,** 1955–1957.

Martin, P. J., 1985: Simulation of the mixed layer at OWS November and Papa with several models. *J. Geophys. Res.,* **90,** 903–916.

——, 1986: Testing and comparison of several mixed-layer models, Naval Oceanographic Research and Development Agency (NORDA) Rep. 143, Naval Research Laboratory, Stennis Space Center, Mississippi, 27 pp.

McWilliams, J. C., P. P. Sullivan, and C.-H. Moeng, 1997: Langmuir turbulence in the ocean. *J. Fluid Mech.,* **334,** 1–30.

Mellor, G. L., 1989: Retrospect on ocean boundary layer modelling and second moment closure. *Proc. Fifth Aha Huliko'a Hawaiian Winter Workshop*, Honolulu, HI, Hawaii Institute of Geophysics, 251–272.

——, and T. Yamada, 1974: A hierarchy of turbulence closure models for planetary boundary layers. *J. Atmos. Sci.,* **31,** 1791–1806.

——, and P. A. Durbin, 1975: The structure and dynamics of the ocean surface mixed layer. *J. Phys. Oceanogr.,* **5,** 718–728.

——, and T. Yamada, 1982: Development of a turbulent closure model for geophysical fluid problems. *Rev. Geophys. Space Phys.,* **20,** 851–875.

Melville, W. K., 1996: The role of surface-wave breaking in air–sea interaction. *Ann. Rev. Fluid Mech.,* **28,** 279–321.

Moeng, C.-H., and J. C. Wyngaard, 1986: An analysis of closures for pressure-scalar covariances in the convective boundary layer. *J. Atmos. Sci.,* **43,** 2499–2513.

Niiler, P. P., 1975: Deepening of the wind-mixed layer. *J. Mar. Res.,* **33,** 405–422.

——, and E. B. Kraus, 1977: One-dimensional models of the upper ocean. *Modelling and Prediction of the Upper Layers of the Ocean*, E. B. Kraus, Ed., Pergamon, 143–172.

Pollard, R. T., 1977: Observations and theories of Langmuir circulations and their role in near surface mixing. *A Voyage of Discovery: George Deacon 70th Anniversary Volume*, M. Angel, Ed., Pergamon, 235–251.

——, P. B. Rhines, and R. O. R. Y. Thompson, 1973: The deepening of the wind-mixed layer. *Geophys. Fluid Dyn.,* **3,** 381–404.

Price, J. F., R. A. Weller, and R. Pinkel, 1986: Diurnal cycling: observations and models of the upper ocean response to diurnal heating, cooling, and wind mixing. *J. Geophys. Res.,* **91,** 8411–8427.

Reed, R. K., 1977: On estimating insolation over the ocean. *J. Phys. Oceanogr.,* **7,** 482–485.

Rotta, J. C., 1951: Statistische theorie nichthomogener turbulenz. *Z. Phys.,* **129,** 547–572.

Skyllingstad, E. D., and D. W. Denbo, 1995: An ocean large-eddy simulation of Langmuir circulation in the surface mixed layer. *J. Geophys. Res.,* **100,** 8501–8522.

Stull, R. B., 1976: The energetics of entrainment across a density surface. *J. Atmos. Sci.,* **33,** 1260–1267.

Tabata, S., 1964: Insolation in relation to cloud amount and sun's altitude. *Studies on Oceanography*, Y. Kozo, Ed., University of Washington Press, 202–210.

——, 1965: Variability of oceanographic conditions at ocean station ''P'' in the northeast Pacific Ocean. *Trans. Roy. Soc. Canada*, Vol. III(Ser. IV), 367–418.

Tandon, A., and S. Leibovich, 1995: Simulations of three-dimensional Langmuir circulation in water of constant density. *J. Geophys. Res.,* **100,** 22 613–22 623.

Terray, E. A., M. A. Donelan, Y. C. Agrawal, W. M. Drennan, K. K. Kahma, A. J. Williams III, P. A. Hwang, and S. A. Kitaigorodskii, 1996: Estimates of kinetic energy dissipation under breaking waves. *J. Phys. Oceanogr.,* **26,** 792–807.

Therry, G., and P. Lacarrère, 1983: Improving the eddy-kinetic-energy model for planetary boundary-layer description. *Bound.-Layer Meteor.,* **25,** 63–88.

Vogelezang, D. H. P., and A. A. M. Holtslag, 1998: Evaluation and model impacts of alternative boundary-layer height formulations. *Bound.-Layer Meteor.,* in press.

Warn-Varnas, A. C., and S. A. Piacsek, 1979: An investigation of the importance of third-order correlations and choice of length scale in mixed layer modelling. *Geophys. Astrophys. Fluid Dyn.,* **13,** 225–243.

Weller, R. A., and J. F. Price, 1988: Langmuir circulation within the oceanic mixed layer. *Deep-Sea Res.,* **35,** 711–747.